

# Signal-based AE characterization of concrete with cement-based piezoelectric composite sensors

Youyuan Lu\*<sup>1</sup>, Zongjin Li<sup>1</sup> and Lei Qin<sup>2</sup>

<sup>1</sup>*Department of Civil and Environmental Engineering, Hong Kong University of Science and Technology, Clear Water Bay, Hong Kong, China*

<sup>2</sup>*Department of Civil Engineering, University of Jinan, Jinan, Shandong Province, China*

*(Received July 4, 2010, Revised December 9, 2010, Accepted December 9, 2010)*

**Abstract.** The signal-based acoustic emission (AE) characterization of concrete fracture process utilizing home-programmed AE monitoring system was performed for three kinds of static loading tests (Cubic-splitting, Direct-shear and Pull-out). Each test was carried out to induce a distinct fracture mode of concrete. Apart from monitoring and recording the corresponding fracture process of concrete, various methods were utilized to distinguish the characteristics of detected AE waveform to interpret the information of fracture behavior of AE sources (i.e. micro-cracks of concrete). Further, more signal-based characters of AE in different stages were analyzed and compared in this study. This research focused on the relationship between AE signal characteristics and fracture processes of concrete. Thereafter, the mode of concrete fracture could be represented in terms of AE signal characteristics. By using cement-based piezoelectric composite sensors, the AE signals could be detected and collected with better sensitivity and minimized waveform distortion, which made the characterization of AE during concrete fracture process feasible. The continuous wavelet analysis technique was employed to analyze the wave-front of AE and figure out the frequency region of the P-wave & S-wave. Defined RA (rising amplitude), AF (average frequency) and P-wave & S-wave importance index were also introduced to study the characters of AE from concrete fracture. It was found that the characters of AE signals detected during monitoring could be used as an indication of the cracking behavior of concrete.

**Keywords:** concrete; fracture; acoustic emission; cement-based piezoelectric composite; wave.

---

## 1. Introduction

In concrete, acoustic emissions (AE) in most cases are generated by the micro or macro crack initiation and propagation. The AE energy released spreads in all directions in the form of broadband elastic waves with a certain kind of radiation pattern identified by the spatial distribution of amplitude and polarization of the first motions. This elastic wave propagated in a concrete can be transformed into electrical signal by cement-based piezoelectric sensors (Lu and Li 2008). And the acquired signals can be used for waveform characteristic analysis by modern signal analysis technique (Grosse 2006). Through bridging the correlation between the features of the AE signals detected and the mechanism of AE sources, the crack or damage process under various kinds of loading conditions can be interpreted and evaluated for early failure warning and life-time assessment (Carpinteri 2006).

---

\* Corresponding author, E-mail: [yylu@ust.hk](mailto:yylu@ust.hk)

Besides early failure warning and life-time assessment which is very helpful in practical engineering, the characterization of the detected AE signal has been drawn more and more attention since it is the exterior manifestation of the condition of AE sources (the micro- or macro- crack of concrete). It helps us indirectly observe micro crack behaviors inside concrete. In literature, people mainly focused on interpreting the behavior of the dipole force, the orientation and movement of the micro-cracks trying to investigate the crack mode during loading process (Ohtsu 1991, Li 1996) on the basis of elasto-dynamics. However, the signal-based characterization of the detected AE signals during damage process used to be restricted due to the capacity limitation of the detection devices in the past decades.

In our research, cement-based piezoelectric composite sensor and the home-programmed DEcLIN health monitoring system were introduced to detect the AE signals generated during three kinds of static loadings with satisfactory resolution and accuracy. The detected and collected AE signals were decomposed into P-wave & S-wave components utilizing the method of wavelet analysis. Based on the analysis results on wave mode, the variation of the AE sources (micro- or macro- crack of concrete) under various kinds of loading condition and fracture processes could be evaluated through the relative variation of weighting ratio of the P-wave & S-wave components. And this information could help us to deeply investigate the micro-crack behaviors of concrete.

## 2. Theoretical background

### 2.1 Wavelet analysis

Continuous wavelet transform (CWT) is introduced to decompose a continuous time waveform function into wavelets. Unlike Fourier transform, CWT possesses the ability to construct a time-frequency representation of an AE signal with very good time and frequency localization.

Considering the capacity of localization of wavelet in time and frequency (i.e. the speed of convergence to 0 of the function  $\psi(t)$  and  $\psi(\omega)$  when the time  $t$  and frequency  $\omega$  tend to infinity) and the regularity, we choose the morlet function as the atoms of transform due to its optimal performance.

$$\psi(t) = Ke^{-t^2/2} e^{i5t} \quad \psi \in L^2(R) \quad (1)$$

Where,  $K$  is a normalization constant used for the reconstruction.

The CWT  $C_f(a, b)$  of the detected time domain signal function  $f(t)$  could be mathematically expressed as

$$C_f(a, b) = \frac{1}{\sqrt{a}} \int_{-\infty}^{+\infty} f(t) \overline{\psi\left(\frac{t-b}{a}\right)} dt \quad a \in R_+ \quad \text{and} \quad b \in R \quad (2)$$

Here,  $\overline{\psi}$  is the complex conjugate of the morlet function.

### 2.2 AE signal characteristic analysis

Three classical fracture modes are Tensile Mode (Mode I Crack), Shear Mode (Mode II Crack) and Tear Mode (Mode III Crack). These modes are sufficient to fully explain the mechanism of fracture behavior. By analyzing the characteristic of the detected AE wave, the fracture modes are

able to be identified based on the knowledge of quantitative seismology theory and methods (Aki and Richards 1980). According to Japan Construction Material Standards, the AE sources from micro-cracking in concrete materials can be classified into tensile crack and shear crack by the characteristic of the detected signals, such as RA value and AF value. RA is short of Rise Time divided by Maximum Amplitude, showing the reciprocal of gradient in AE waveform, and owning a unit of ms/V. AF is used as quantitative estimation on the majority of frequency content contained in AE signals.

$$RA = \frac{t_r}{A_p} \quad (3)$$

$t_r$  refers to the time period required for a signal to change from 10% to 90% of maximum voltage amplitude of its waveform.

$A_p$  refers to the maximum voltage amplitude of a signal waveform.

$$AF = \frac{N}{t_d} \quad (4)$$

$N$  refers to the number of times AE waveform crossing pre-set threshold.

$t_d$  represents the duration of AE waveform.

Tensile cracks are supposed to have relatively high AF value and small RA value, while shear cracks to be just opposite. Recently, a number of experiments were performed attempting to distinguish different crack modes in concrete materials by utilizing two parameters (Ohtsu and Tomoda 2008). In this study, signal-based waveform characteristic parameters of each individual AE signal recorded in the different stages of loading or damage are calculated using Eqs. (3) and (4), and then the statistical distributions of AR and AF of AE signals are displayed in a planar graph for comparison. It is expected that the signal characteristics have a close relationship with wave mode and AE sources. By analyzing the distribution region and trend, AE source and micro-crack conditions are further studied.

### 2.3 Signal-based fracture energy index

Since AE signal is usually considered as a function of varying amplitude through time, it seems reasonable to use the area under the  $f(t)$  enveloping curve as a good approximate measurement of the energy of an AE signal. The total energy of a signal  $f(t)$  is thus defined as the sum of squared module

$$\varepsilon_f = \sum_{t=0}^{\Delta N-1} |f(t)|^2 \quad (5)$$

$t$  refers to the discrete time point of the detected signal.

$N$  represents the total number of the discrete time points.

In digital signal processing, physical unit of the signal energy is routinely discarded, and signals are renormalized whenever convenient. Therefore, the norm of a signal  $f(t)$  is introduced as the square root of its total energy

$$\|f(t)\| \triangleq \sqrt{\varepsilon_f} = \sqrt{\sum_{t=0}^{N-1} |f(t)|^2} \quad (6)$$

Where,  $\|f(t)\|$  can be regarded as the absolute value or radius of a vector to scale the fracture energy released during damage process, although, it is not the exactly fracture energy released but a customized index of the fracture energy based on the relationship between fracture energy and AE signal energy detected (Landis 2002 and Prasad 2008).

### 3. Experimental detail

#### 3.1 Cement-based piezoelectric composite sensors array

From previous results (Lu and Li 2008), the compatibility of the piezoelectric material and matrix material is a critical issue since it greatly affects the performance of the piezoelectric material in its ability of detection and actuation. If the compatibility can not meet the request, the detecting sensitivity and SNR (signal to noise ratio) will be unsatisfactory in health monitoring. In civil engineering, concrete is dominant construction material. However, there exists relatively large difference on the acoustic impedance between concrete and piezoelectric material. Traditional sensors which are especially designed for metal structures may not be suitable for concrete material for achieving optimal performance. In 2002 Li *et al.* found that it was possible to overcome these problems using cement-based piezoelectric composite material which has the acoustic impedance value (around 10 Mrayl) close to that of the concrete matrix (8.64 Mrayl) by adjusting the mixture proportion of ceramic material and portland cement. It was found that the backing material supporting the piezoelectric sensor has a great influence on its damping characteristics. With an active piezoelectric material of acoustic impedance similar to that of the backing material (concrete), it will produce the

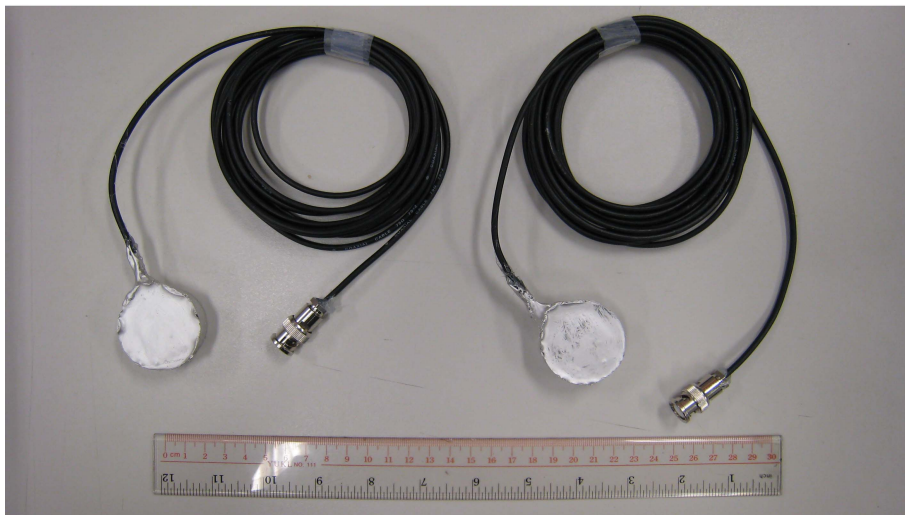


Fig. 1 Cement-based piezoelectric composite sensor of 0-3 connectivity pattern

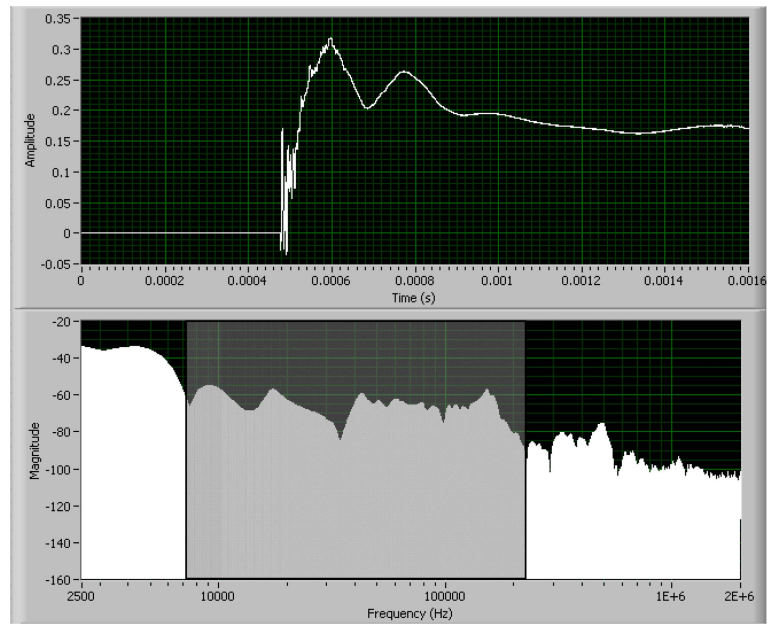


Fig. 2 Calibration curve of cement-based piezoelectric sensor (top: time domain response, bottom: frequency domain response)

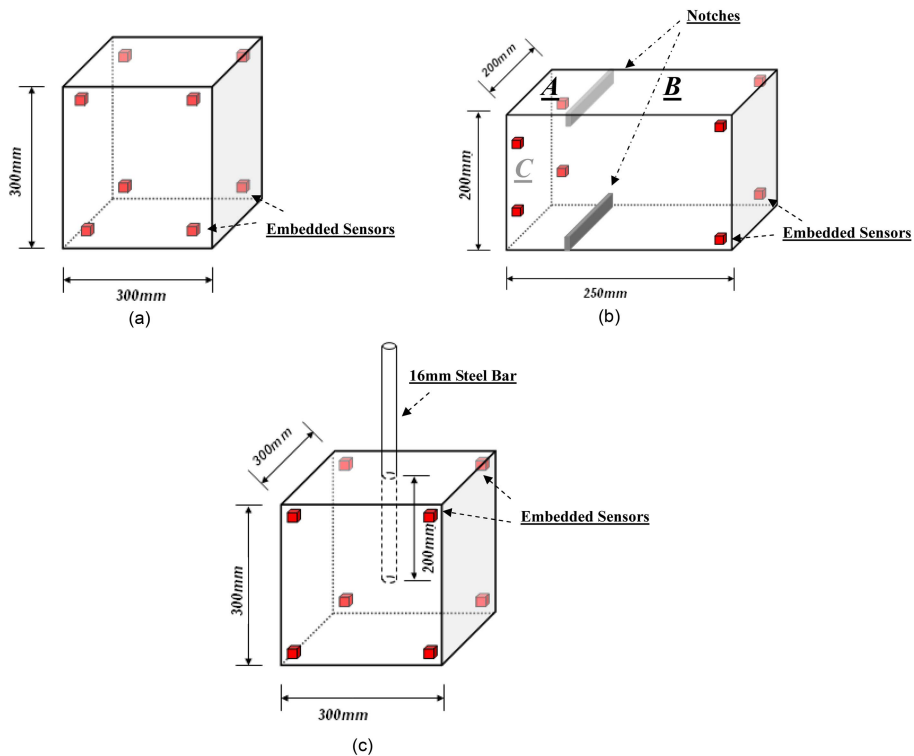


Fig. 3 (a) Detecting array arrangements for Cubic-splitting test, (b) detecting array arrangements for Direct-shear test and (c) detecting array arrangements for Pull-out test

most effective damping. Such a piezoelectric sensor will produce an approximately flat and wide bandwidth resulting in higher sensitivity when embedded into concrete. Further more, coupling defect would be greatly improved by embedding cement-based composite material into concrete, and AE energy transforming efficiency will be increased due to the minimum AE wave reflection along the medium interface. Therefore, the SNR will be enhanced accordingly. Nowadays, cement-based piezoelectric composites with six kinds of connectivity patterns have been developed. In this experiment, cement-based piezoelectric composites of 0-3 connectivity patterns were employed as constituent material of the piezoelectric sensor (see Fig. 1). The frequency domain calibration curve is shown in Fig. 2. It can be figured out that an approximately flat and wide bandwidth existed within the frequency region from 8 kHz~200 kHz. Totally eight piezoelectric sensors were embedded in all the corners of the concrete specimens (see Fig. 3) to constitute the detecting array for health monitoring of concrete specimens during static loading. In these experiments, at least 5 sensors (or 4 un-coplanar sensors) were required to localize the AE sources correctly and satisfactorily. A smart C++ program was coded to carry the job.

### 3.2 Home-programmed DEcLIN health monitoring system

The elementary function block of the DEcLIN system is illustrated in Fig. 4. The system consists of cement-based piezoelectric sensors presented previously, voltage pre-amplifier, 8-channel data acquisition hardware and software.

The commercially available Germany-made voltage amplifier (49 dB gain changeable) was used to amplify the Micro-Volt signals into Mill-Volt signals. The analog input DAQ hardware in the block diagram is an 8-channel 12 bit resolution signal acquisition card. The maximum sampling rate is 10 MHz which is capable of reconstructing the signals within 2 MHz frequency region with negligible distortion. The software is divided into two components, signal acquisition software and post-analysis software, to efficiently prevent the interference between two individual processes. Advanced signal-based health monitoring analysis, together with traditional parameter-based health monitoring analysis, can be realized based on provided system framework. In the acquisition software, the program identifies a genius AE event by pre-set threshold trigger. The threshold level is manually set by evaluating the background noise level ahead of health monitoring. In our experiments, the threshold level is set to be 0.01V which is just beyond the background noise level. After being triggered, 8000 points data (0.2  $\mu$ s time interval) will be recorded with 30% pre-trigger data points and 70% post-trigger data points. The parameters (number of recording, triggering level, number of channels, data length, and sampling rate) of monitoring can be pre-set according to the goal and requirement of a practical task. The software profile can display the current 8-channel signal waveforms and related parameter diagrams (accumulated event number and event rate vs. time) in real time.

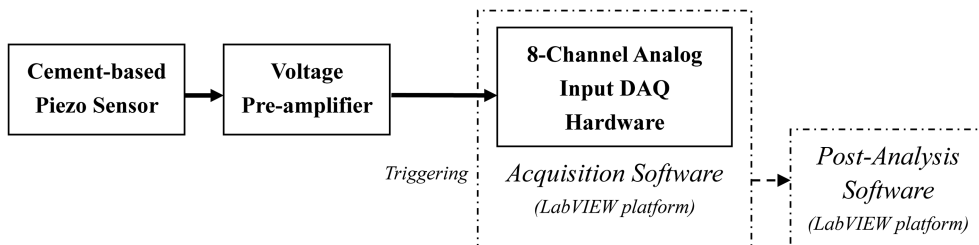


Fig. 4 Block diagram of DEcLIN monitoring system

### 3.3 Experimental setup

#### 3.3.1 Cubic splitting test

The objective of Cubic-splitting test was to induce a tensile-crack dominant failure mode on concrete specimen. The detected AE signals by cement-based piezoelectric sensors during test could be used to extract the signal-based information on the fracture process for post-analysis of the AE sources (i.e. micro-cracks). The test procedure and apparatus were designed conforming to ASTM C496-96, while the dimension of concrete specimen is a 300 mm×300 mm×300 mm cube (see Fig. 3(a)) which is convenient for embedding sensors in the eight corners to form a detection array. The mixture proportions used in preparing the specimens (Cubic-splitting, Direct-shear and Pull-out) are listed in Table 1.

Two LVDTs of 10 mm working range were mounted on the front and back side of the concrete cube in horizontal direction respectively to measure the horizontal displacement due to expansion in the center. The displacement values from LVDTs were also fed back to control the loading rate for guaranteeing a stable loading process. When compressive force is applied on the top and bottom center line of the specimen, micro-cracks were expected to occur in the central region with high tensile stress. After that, a major tensile crack was formed when the load applied approached the maximum loading capacity of the concrete specimen.

#### 3.3.2 Direct-shear test

The objective of Direct-shear test was to induce a shear crack dominant failure mode on concrete specimen. Similarly, AE detection by embedded cement-based piezoelectric sensors was carried out throughout the test. ASTM standard D5607-02 was used as reference for apparatus and test procedure design. The dimension of concrete specimen is a 250 mm long, 200 mm wide and 200 mm high cuboid. A 40 mm deep and 2.5 mm wide notches were pre-set vertically inside both the top and bottom faces of the cuboid with a distance of 50 mm to the face C (see Fig. 3(b)). The cement-based piezoelectric sensors array arrangement is slightly different from the rest of the tests due to the presence of induced notches and large compressive stress on the face A. The four sensors supposed to be at the corners right below face A were embedded with a distance of 40mm for safety and reliability. The shear mode crack was expected to firstly occur at the tip of the induced notches when a compressive force was applied on the face A vertically, while the face B and its opposite face were both tightly restricted by a couple of flat steel plates with a bunch of high yield steel bars connected. LVDTs of 25 mm working range were installed on the top of the concrete cuboid to measure the vertical downward displacement relative to the stationary reference plate of the loading machine. The displacement values from LVDTs were fed back to control the loading rate for guaranteeing a stable loading process similar to that of Cubic-splitting test.

#### 3.3.3 Pull-out test

The objective of Pull-out test was to study the process of debonding and concrete micro-cracks surrounding the interface of concrete and steel bar due to slip. ASTM standard C900-94 was used

Table 1 The mixture proportion of the concrete specimen in the experiments

Concrete type	Cement	Water	Fine aggregate	SP (ADVA 105)
Mortar	1	0.5	1.8	0.2%

as a guideline for apparatus and test procedure design. The dimension of concrete specimen was the same with that of Cubic-splitting test for the convenience of embedding the cement-based piezoelectric sensors array (see Fig. 3(c)). A 16 mm diameter round steel bar was embedded into the concrete specimen with a depth of 200 mm in the central axis. Debonding and cracking were expected to occur at the interface between concrete material and steel bar when a pull out force applied on the exposed part of the steel bar was sufficient large. LVDTs of 25 mm working range were installed on the top side of the concrete cube to measure the vertical displacement of the steel bar relative to the stationary reference plate of the apparatus. Close loop control was applied to guarantee stability of loading process.

#### 4. Classification of wave mode in acoustic emission signals

In AE, little information is available on the P-wave and S-wave characterization on AE signals from concrete cracking. On the basis of seismology, the velocity of S-wave is around 60% of that of P-wave. In our experiments, Cubic-splitting test for instance, by estimating the propagation distance of AE signals and velocity difference, the TDOA (time difference of arrivals) of P-wave & S-wave shall be in the range of 0.077 ms~0.12 ms given that P-wave acoustic speed in concrete is within 3100~4200 m/s (Li and Shah 1994). Therefore, a wave mode completed separation region is expected to exist at the wave-front of detected AE signals. By analyzing the wave-front, the characteristics of P-wave & S-wave are able to be pointed out. CWT was employed as a useful tool to investigate the potential wave mode completed separation region. The wavelet transform is a linear operation that decomposes a signal into a set of frequency channels. The decomposition completely characterizes the AE signals in both time and frequency domain. Basically, it could be regarded as the 2-D FFT transform.

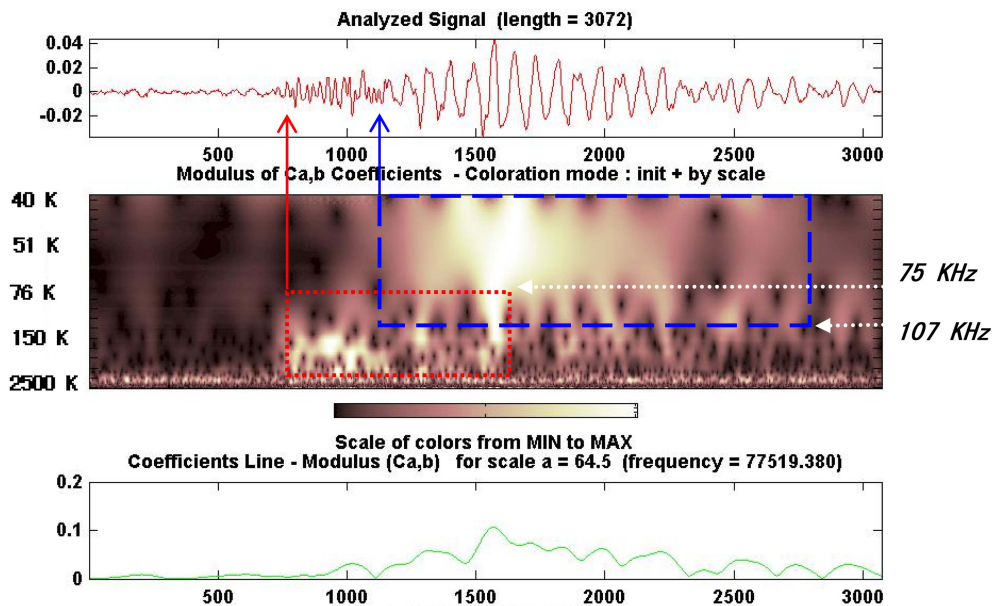


Fig. 5 CWT of a typical AE waveform from Cubic-splitting test

Fig. 5 illustrates the coloration mode diagram of modulus of  $C_{a,b}$  coefficients with dark area representing low value and light area representing high value. From the wavelet transform diagram of a typical AE signal waveform, we could clearly observe that high frequency components (82 kHz~332 kHz highlighted in the dot line box of Fig. 5) arrived ahead of other frequency components, which is consistent with the arrival time of the wave-front. They were followed by a bunch of low frequency components (45 kHz~93 kHz highlighted in the dash line box of Fig. 5) with a time difference of 0.84 ms~0.1 ms (roughly 420~500 discrete data points of sampling period  $2 \times 10^{-7}$ s). Thus, this TDOA conform to the fact that the velocity of S-wave is 60% of that of P-wave regardless the condition of the AE sources and propagation medium. And the frequency components in the dot line box indicated in the Fig. 5 belongs to the P-wave component of the AE waves. Similarly, the frequency components in the dash line box belong to the S-wave component of the AE waves. Through the statistics of population characteristics by inference from sampling, it was found that S-

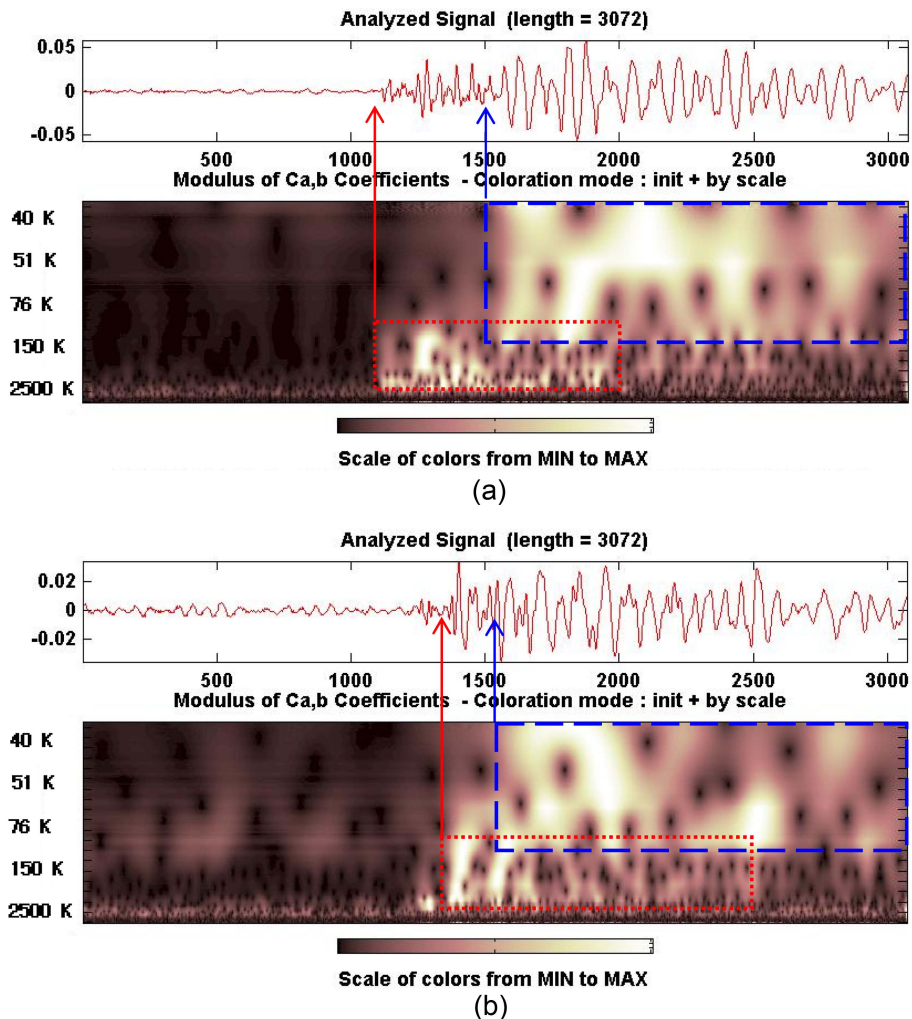


Fig. 6 (a) CWT of a typical AE waveform from Direct-shear test and (b) CWT of a typical AE waveform from Pull-out test

wave mainly covered the frequency region of 39 kHz~107 kHz, while P-wave mainly covered the region of 75 kHz~333 kHz in the AE signals from concrete cracks. The two wave modes like two independent bands with overlapping band in the frequency region of 75 kHz~107 kHz. Hence, the average frequency of P-wave is naturally expected to be higher than that of S-wave. Furthermore, the two independent bands always existed as necessary components of AE signals from concrete cracks and delaminating regardless of the types of fracture or the processes of the loading (see Figs. 6(a) and 6(b)).

Despite of the fact that the AE waves from concrete cracks are mixed mode mechanical waves, digital band-pass filter can be used to filter out the P-wave or S-wave component of an AE wave to further study the characteristics of the previous estimation of frequency regions. In this work, two 5-order Butterworth band-pass filters having central frequency of 60 kHz and 200 kHz with hamming moving average window were chosen to filter out pure P-wave & S-wave components, respectively, as results shown in Fig. 7. It can be seen that the RA value of 60 kHz center frequency filtering results is roughly 2.7 times higher than that of 200 kHz center frequency filtering results. Alternatively, we could select a special frequency channel (i.e. the modulus of  $C_{a,b}$  coefficients at a specified frequency) of the wavelet transform diagram, to investigate the variations of coefficients line in time domain. Here, we select two frequency channels on 55.2 kHz (S-wave) and 208.3 kHz (P-wave) for illustration (see Figs. 8(a) and 8(b)). For 55.2 kHz coefficient line, RA value (i.e. the slope indicated in the corresponding diagram of Fig. 8(b)) is  $3.56 \times 10^{-3}$ , which is much larger than the value of  $1.2 \times 10^{-3}$  obtained from 208.3 kHz coefficient line (see Fig. 8(a)). Following the same calculation procedure from sampling population, we could discover exactly the same feature in all the cases no

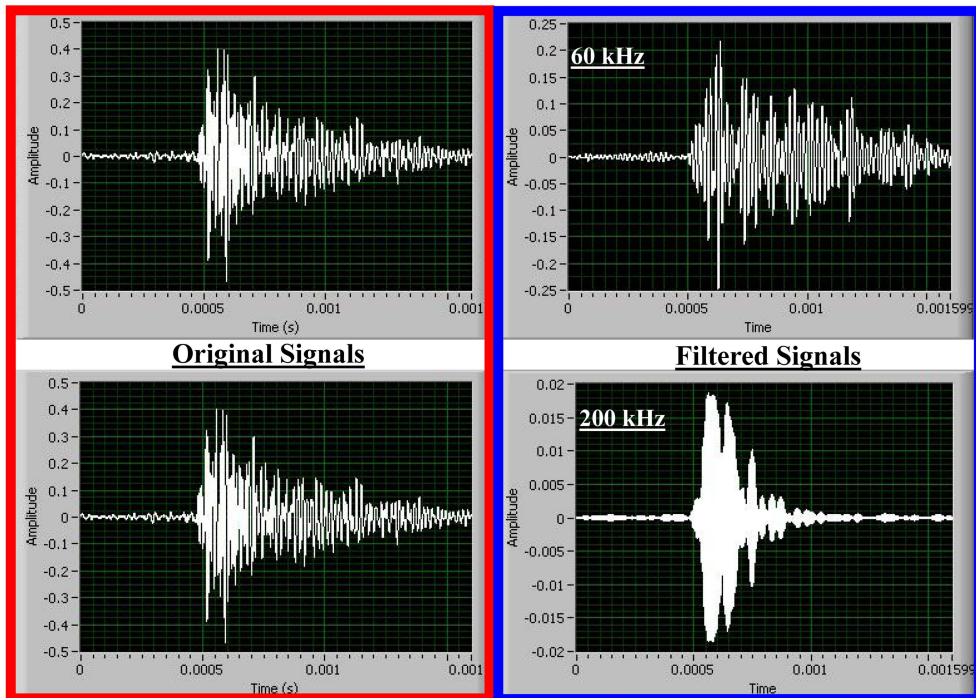
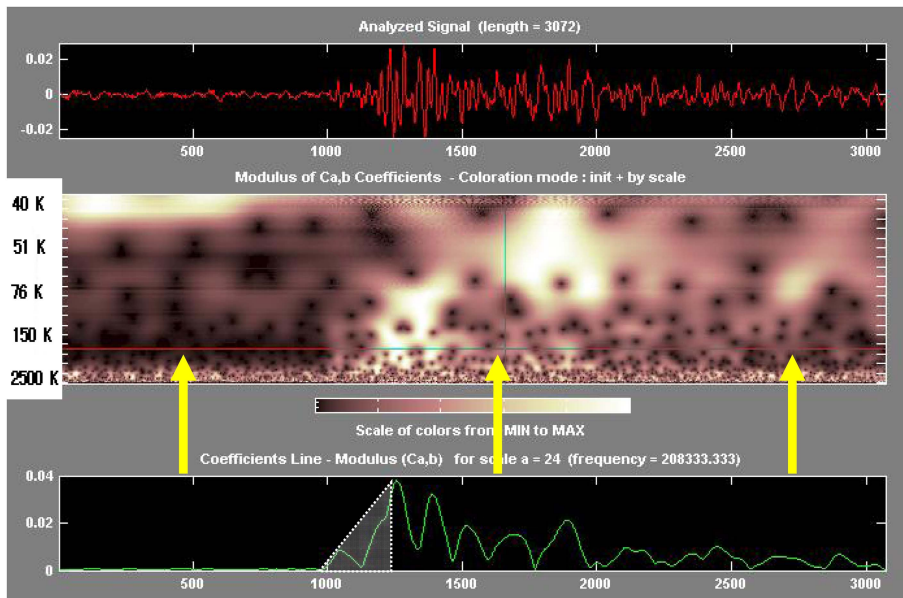
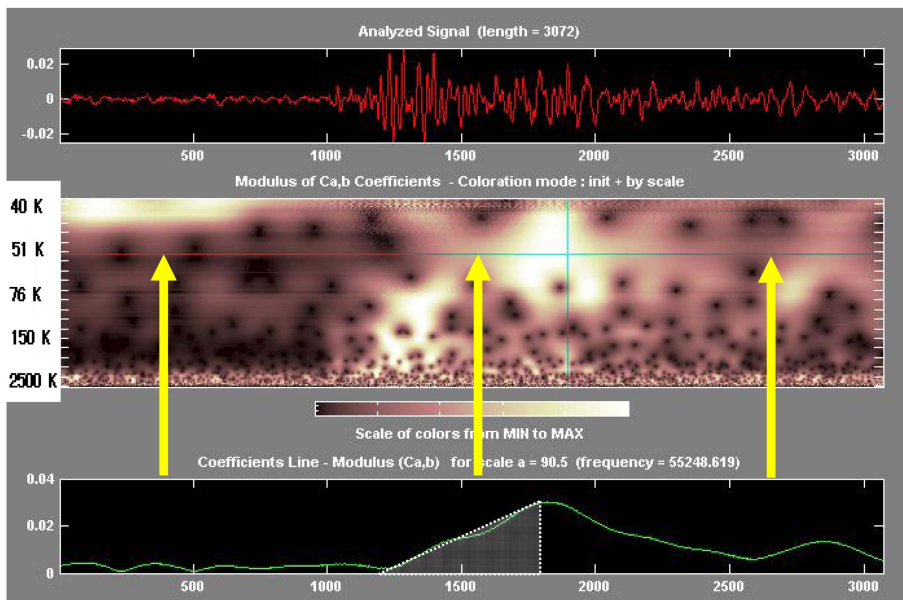


Fig. 7 Band-pass filtering (top is 60 kHz and bottom is 200 kHz)



(a)



(b)

Fig. 8 Coefficient line for a specified, scale in CWT results (yellow arrows pointing the coefficient lines on (a) 208.3 kHz and (b) 55.2 kHz)

matter where the samples came from. As mentioned previously, the RA value and AF value are used as the crack classification standard in JCMS (see Fig. 9). From these two parameters, cracks are readily classified into tensile crack in the upper left corner and shear crack in the lower right corner of the diagram. The tensile crack is found to have relative small RA value but large AF,

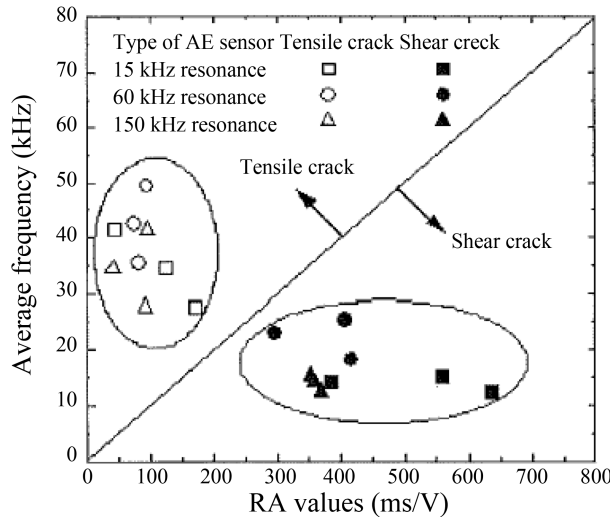


Fig. 9 Classification of cracks by AE characteristic in JCMS

while the shear crack has relative large RA value and small AF, which is consistent with the features of P-wave & S-wave components, respectively, from the results of band-pass filtering and single frequency channel wavelet analysis. Therefore, it implies that a close relationship bridging wave mode and crack mode may exist. And P-wave is more likely to be correlated to the tensile crack, while S-wave is more likely to be correlated to the shear crack. Therefore, RA and AF features might also be used to distinguish the distribution of P-wave and S-wave in different loading processes.

### 5. The variation of P-wave & S-wave components during loading process

As stated previously, the AE waves from concrete cracks belong to generalized scope of mixed mode wave. The P-wave & S-wave components of each signal never disappear (generalized mixed mode) regardless of failure type and loading process. However, the energy weightings of each wave mode contained in individual AE were not kept the same in different fracture types and loading processes. Here, assuming that the S-wave & P-wave components do not overlap in frequency domain and only P-wave & S-wave are involved in for simplicity, we define the importance index (of a certain wave mode) as the signal energy index ratio of a certain wave mode to the signal energy index of the entire single AE signal formulated in Eq. (7).

$$\varphi_i = \frac{\|f_i\|}{\|f\|} = \frac{\sqrt{\varepsilon_{fi}}}{\sqrt{\varepsilon_f}}, \quad (0 < \varphi_i < 1, \text{ valid if only P-wave \& S-wave involved}) \quad (7)$$

Here,  $f_i$  and  $\varepsilon_{fi}$  is the time function and the sum of squared module of  $p$  or  $s$  wave mode component,  $f$  and  $\varepsilon_f$  is the time function and the sum of squared module of the detected original wave. Based on the assumption stated above, we can easily get  $\varphi_p + \varphi_s = 1$  according to the Parseval's Theorem.

Figs. 10-12 shows the distribution  $\varphi_p$  and  $\varphi_s$  of randomly selected AE samples in each loading

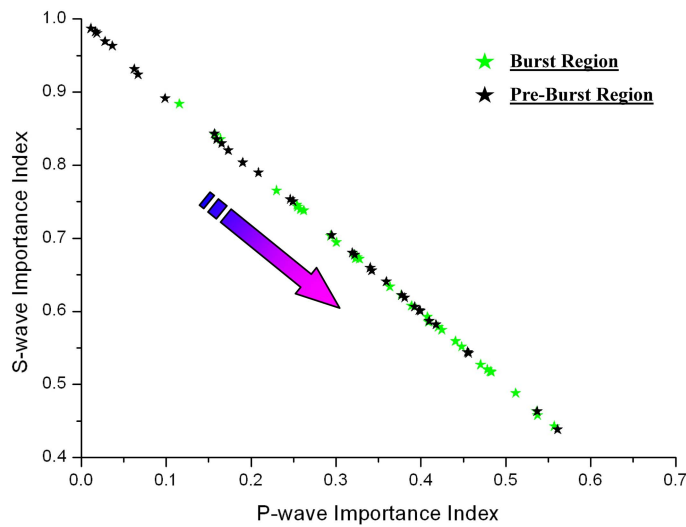


Fig. 10 Importance index of AEs in Cubic-splitting test

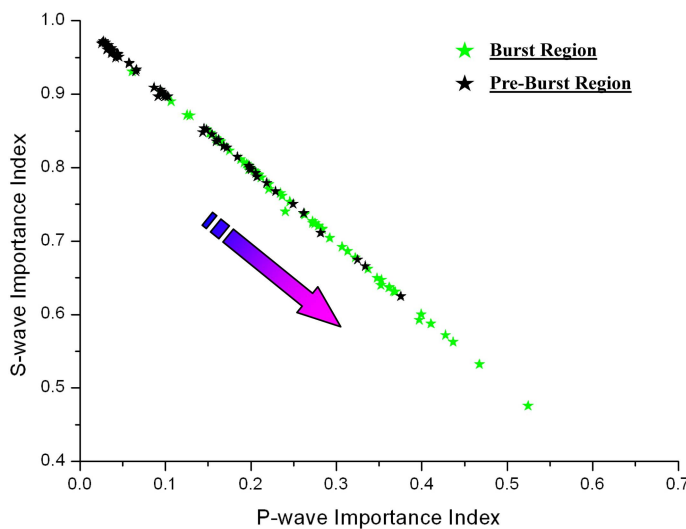


Fig. 11 Importance index of AEs in Direct-shear test

stage. Herein, if P-wave mode importance index  $\varphi_p$  is increased to a certain level, this signal is likely to be a P-wave rather than S-wave since the characteristics of P-wave tend to be stronger, while the characteristics of S-wave become weaker and even gradually submerged comparatively. Simply speaking, P-wave components account for relatively more energy weighting (not necessarily 50% because cement-based piezoelectric sensor owns different sensitivities to P-wave & S-wave) in the individual AE, and AEs thus turn to distribute towards bottom right corner of the figures. As a result, the AE signal tends to bear a typical P-wave. Similarly, some of the signals would also be more likely to be recognized as S-wave depending on the S-wave mode importance index  $\varphi_s$ , and distribute towards top left corner of the figures.

Considering the piezoelectric sensors with various kinds of polarization direction and vibration

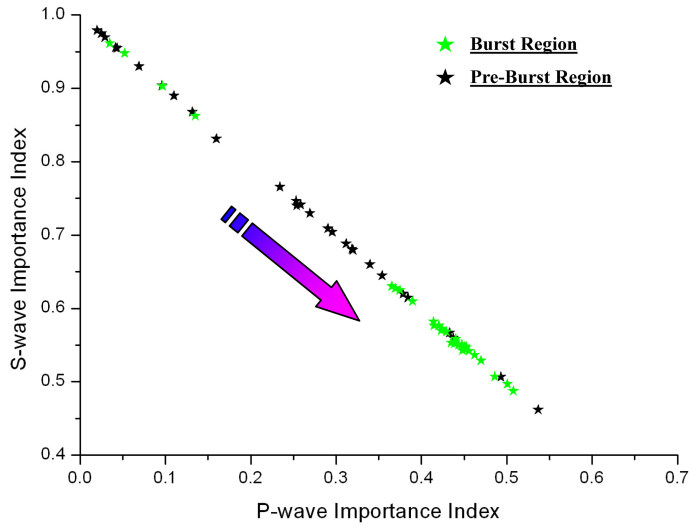


Fig. 12 Importance index of AEs in Pull-out test

direction will have different sensitivity to P-wave & S-wave respectively. Therefore, it is more meaningful to care about the relative variation of P-wave & S-wave components importance index ratio instead of absolute value. And the relative variation of single wave mode energy weighting (i.e. the relative variation of importance index) within the loading process could be used to reflect the change of micro-crack behavior during concrete fracture. As illustrated in Figs. 13-15, the RA and AF variations in all the tests and loading processes were also illustrated to distinguish the statistical distribution of wave mode. Each dot on the figures shows the RA and AF distributions of a corresponding AE signal. And the loading processes were divided into pre-burst and burst region by the time point when AEN (accumulated event number of AE) and ER (the event occurring rate

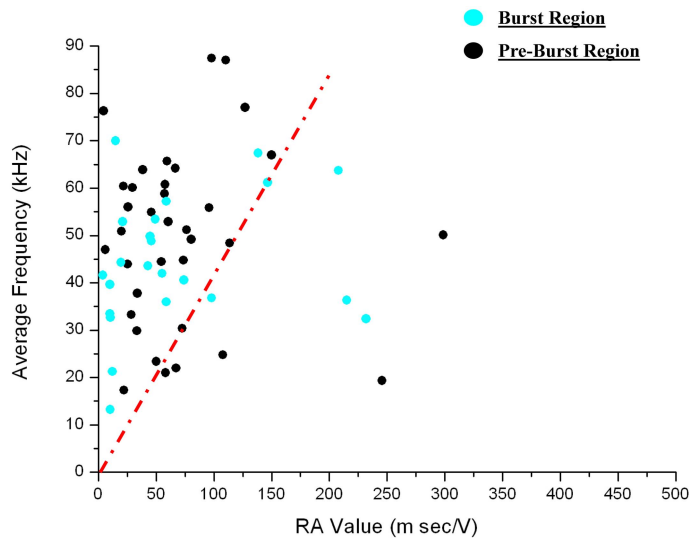


Fig. 13 Distribution of AF & RA in Cubic-splitting test

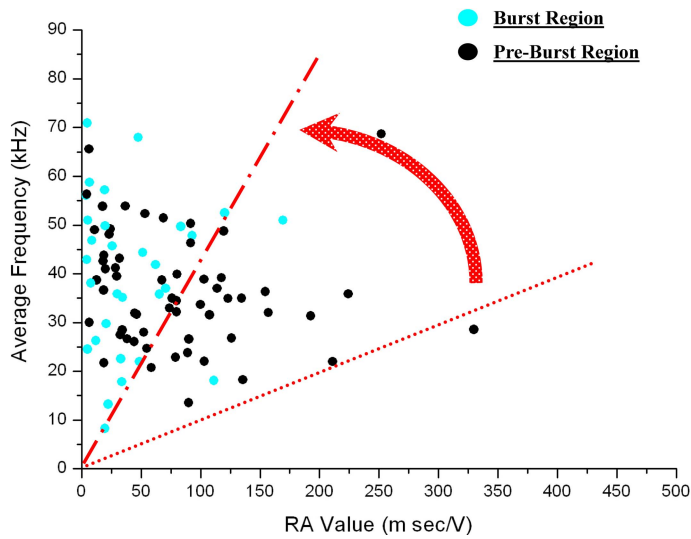


Fig. 14 Distribution of AF & RA in Direct-shear test

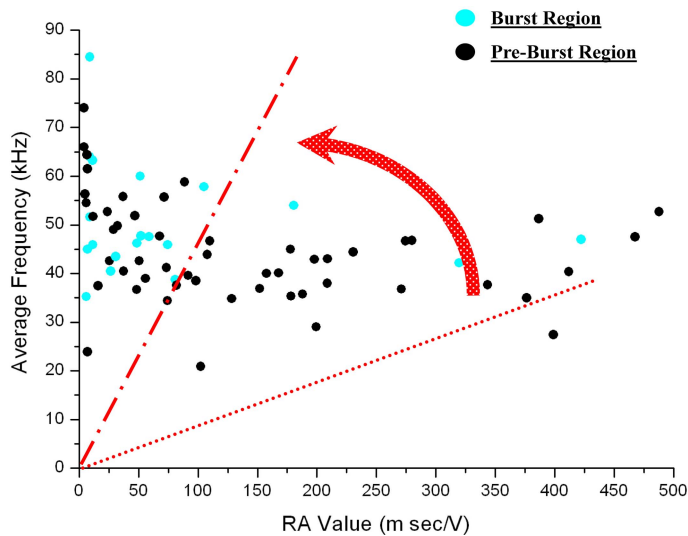


Fig. 15 Distribution of AF & RA in Pull-out test

of AE) both started to increase significantly (Lu *et al.* 2010), indicating a rapid burst of AE signals.

Dash dot lines were drawn on Figs. 13-15 to standardize the transition boundary of distribution areas with exactly the same slope ( $AF/RA=0.4$ ) through origin highlighting the difference in distribution features between each figure. Compared to that of Direct-shear test and Pull-out test, Fig. 13 shows that most of dots were massed up in the region of  $AF/RA > 0.4$  in the Cubic-splitting test regardless of loading stages. AF relatively uniformly distributed in the range of 14 kHz~86 kHz, and RA mainly distributed in the range of 0~156 msec/V. It seems that the variation of distribution is not obvious. Yet it could be more clearly seen that importance index distribution turned to slightly move towards bottom right corner during burst region when applied load reaching 82% of ultimate load

up to failure (see Fig. 10). The median value of P-wave importance index was observed being increased from 0.255 to 0.383. In Direct-shear test, although AEs distributed over a wider region of  $AF/RA > 0.1$  illustrated in Fig. 14 (AF uniformly distributed in the range of 12 kHz~71 kHz, and RA value mainly distributed in the range of 0~200 m sec/V), detected signals turned out to concentrate into the P-wave or pro-P-wave area above the transition boundary during the defined burst region featured applied load reaching 96% of ultimate load up to failure with ER increasing dramatically by over 20 times. And the results of wave mode importance index (see Fig. 11) again prove that AE in the burst region turned to have more P-wave energy weighting compared to the rest of AE. The moving trend could be more clearly figured out in Direct-shear than in Cubic-splitting given that the median value of P-wave importance index was observed being increased from 0.12 to 0.261. In Pull-out test (see Fig. 15), AEs initially distributed in the region of  $AF/RA > 0.1$  as that of Direct-shear (see Fig. 14). AF densely distributed in the range of 27 kHz~66 kHz, and RA distributed in the range of 0~500m sec/V. However, AEs were found to concentrate into the pro-P-wave area above  $AF/RA=0.4$  in burst region (see Fig. 15). And Fig. 12 indicated that the median value of P-wave importance index significantly increased from 0.274 to 0.39 during burst region.

## 6. Angle difference model

Landis in 1995 found that the wave mode had a close relationship with the angle between a vector normal to the micro-crack plane and a vector representing the direction of crack motion of one face relative to the other based on the moment tensor estimation. A shift in the dominant mechanism of micro-crack was observed during the fracture process of mortar.

It is widely accepted that concrete is more sensitive to tensile fracture than to shear fracture. Tensile fracture always dominates as long as the tensile stress is present (Vonk 1993). Here, an adequate tiny cubic element in Direct-shear test was assumed and taken for explanation. The stress condition could be regarded as a plane stress condition (see Fig. 16). And compression stress and shear stress were applied on the corresponding surfaces. The element was very likely to have a

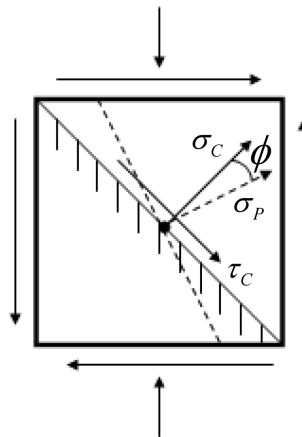


Fig. 16 Illustration of angle difference (broken line represents the principal plane of stress, solid line represents the actual crack plane)

micro-crack plane normal to the principal stress direction. If only normal tensile stress  $\sigma_p$  existed on the micro-crack plane (broken line vector on the principal plane of stress in Fig. 16), a dynamic displacement in the same direction of the tensile step force was generated with the largest amplitude considering the Green's function and the radiation pattern of P-wave & S-wave (Ohtsu 1987). Meanwhile, the amplitude of a dynamic displacement in the direction perpendicular to the step force was not high enough to affect the characteristic of P-wave. Simply speaking, the characteristics of P-wave mode were probably able to be clearly detected by our cement-based piezoelectric sensors, leading to relatively high P-wave mode energy weighting in an AE and consequently relatively large AF and small RA. Therefore, the time period with distinctive P-wave characteristics were theoretically resulted from the fact the micro-crack plane was strictly perpendicular to the direction of principal tensile stress direction. Because the concrete materials itself is a very complex system containing voids, needle-like crystal and irregular solid particle, the ideal condition of micro-crack could seldom been found in actual situation. Mostly, it is believed that the plane of micro-crack ought to have a certain angle difference  $\phi$  with the principal tensile stress direction (see Fig. 16). From the knowledge of mechanics of materials, the difference of direction angles will cause an additional shear force  $\tau_c$  along the micro-crack plane. And the shear force along the micro-crack plane was likely to excite a dynamic displacement in the direction of slippage of the micro-crack plane. Therefore, the characteristics of S-wave would become much clearer in most radiation directions, leading to relatively high S-wave mode energy weighting and consequently relatively small AF but large RA. Therefore, if the angle difference between the principal tensile stress direction and micro-crack plane is small enough (i.e. approach pure tensile crack mode), AE detected will be close to that of P-wave. Otherwise (i.e. shear mode), AE detected will approach a typical S-wave.

Despite of different types of crack modes, the detected AE signals from micro-cracks of concrete materials were observed to approach the signal character of P-wave mode when the load level was close to the ultimate load to a certain degree at the same time the ER of AE started to increase rapidly (i.e. in the period of burst region), and the P-wave importance indices  $\varphi_p$  were also found to be increased correspondingly. Associated with related study on 3-D localization of AE in each test (Lu *et al.* 2010), the AE burst regions occurred at the same time when the micro-crack localization phenomena occurred. Based on the fact tensile crack theoretically own more P-wave mode energy weighting (i.e. high P-wave importance index), micro-cracks during micro-crack localization period approached in pure tensile crack mode. Therefore, the angle differences were observed to be decreased to some extent in the localization period; however, before micro-crack localization the angle difference was likely to be randomly distributed in a wider region. And the increasing in P-wave importance index was a direct consequence of the reduction in angle difference during burst region. In Cubic-splitting, the reduction in angle difference is relatively small compared to Direct-shear and Pull-out tests.

## 7. Conclusions

In this paper, signal-based characterization of AE signals was performed using cement-based piezoelectric composite sensors and home-programmed AE monitoring system. The detected signals were successfully decomposed into P-wave & S-wave components by CWT. And based on the signal-based analysis of AE signals, the micro-crack behaviors of the concrete during static loading were investigated. The following conclusions can be drawn from the study.

1. By using the cement-based piezoelectric composite sensors, the AE signals generated from the micro-cracking and macro-cracking of concrete can be clearly detected with high sensitivity and SNR. The detected signals carry adequate information of the damage processes of concrete specimens under various kinds of static loadings.

2. Continuous wavelet analysis is useful in investigating the P-wave & S-wave components of an individual AE signal resulted from concrete cracking. It is found that S-wave mainly cover the frequency region of 39 kHz~107 kHz, while P-wave mainly cover the region of 75 kHz~333 kHz with overlapping band in the frequency region of 75 kHz~107 kHz. Both P-wave & S-wave components exist in all the AE signals detected.

3. By analyzing the characteristic of each wave mode component in AEs, it is found that P-wave mode component owns similar signal characters with AE from tensile crack, while S-wave mode component owns similar signal characters with AE from shear crack based on the knowledge of JCMS standard.

4. P-wave & S-wave importance indices of AE signal are helpful in studying the relative variation of the P-wave & S-wave energy weighting. The distributions of AF and RA values are able to provide additional information on the variations of signal-based characters of AEs during concrete fracture processes. The AEs occurred within defined burst region turn out to hold more P-wave energy weighting.

5. The angle difference model is able to correlate the increasing in P-wave energy weighting to the reduction of angle difference of micro-crack plane.

## Acknowledgements

The financial supports from Ministry of Science & Technology under grant of 2009CB623200 and Hong Kong Research Grant Council under grant of N\_HKUST 637/09 are greatly acknowledged.

## References

- Burrus, C., Gopinath, R. and Guo, H. (2005), *Introduction to wavelets and wavelet transforms: a primer*, Pearson Education Limited.
- Carpinteri, A., Lacidogna, G. and Pugno, N. (2007), "Structural damage diagnosis and life-time assessment by acoustic emission monitoring", *Eng. Fracture Mech.*, **74**, 273-289.
- Finck, F., Yamanouchi, M., Reinhardt, H. and Grosse, C. (2003), "Evaluation of mode I failure of concrete in a splitting test using acoustic emission technique", *Int. J. Fract.*, **124**, 139-152.
- Grosse, C. and Finck, F. (2006), "Quantitative evaluation of fracture processes in concrete using signal-based acoustic emission technique", *Cement Concrete Compos.*, **28**, 330-336.
- Grosse, C., Reinhardt, H. and Finck, F. (2003), "Signal-based acoustic emission techniques in civil engineering", *J. Mater. Civil Eng.*, **15**(3), 274-279.
- JCMS-III B5706 (2003), *Monitoring method for active cracks in concrete by acoustic emission*, Federation of Construction Materials Industries, Japan.
- Landis, E. and Baillon, L. (2002), "Experiments to relate acoustic emission energy to fracture energy of concrete", *J. Eng. Mech.*, **128**(6), 698-702.
- Landis, E. and Shah, S. (1995), "The influence of micro-cracking on the mechanical behavior of cement-based materials", *Adv. Cement Based Mater.*, **2**, 105-118.
- Li, F. and Li, Z. (2000), "Acoustic emission monitoring of fracture of fiber-reinforced concrete in tension", *ACI*

- Mater. J.*, **97**(6), 629-636.
- Li, Z. (1996), "Micro-crack characterization in concrete under uniaxial tension", *Mag. Concrete Res.*, **48**(176), 219-228.
- Li, Z. and Shah, S. (1994), "Localization of micro-cracking in concrete under uniaxial tension", *ACI Mater. J.*, **91**(4), 372-381.
- Lu, Y. and Li, Z. (2008), "Cement-based piezoelectric sensor for acoustic emission detection in concrete structures", *Proceedings of the 11th International Conference on Engineering, Science, Construction, and Operations in Challenging Environments*.
- Lu, Y., Li, Z. and Qin, L. (2011), "Signal-based AE monitoring on mortar with cement-based piezoelectric sensors", *ACI Mater. J.*, **108**(2), 178-186.
- Misiti, M., Misiti, Y., Oppenheim, G. and Poggi, J. (2007), *Wavelets and their applications*, ISTE Ltd.
- Niwa, Y., Ohtsu, M. and Shiomi, H. (1981), "Waveform analysis of acoustic emission in concrete", *Memoirs of the Faculty of Eng., Kyoto Univ. MEKYA*, **63**(IV), 319-330.
- Ohtsu, M. (1987), "Mathematical theory of acoustic emission and its application", *J. Soc. Mater. Sci.*, **36**(408), 1025-1031.
- Ohtsu, M. (1996), "The history and development of acoustic emission in concrete engineering", *Mag. Concrete Res.*, **48**(17), 321-330.
- Ohtsu, M. (2006), "Quantitative AE techniques standardized for concrete structure", *Adv. Mater. Res.*, **13-14**, 183-192.
- Ohtsu, M. and Tomoda, Y. (2008), "Phenomenological model of corrosion process in reinforced concrete identified by acoustic emission", *ACI Mater. J.*, **105**(2), 194-199.
- Ohtsu, M., Shigeishi, M., Iwase, H. and Koyanagi, W. (1991), "Determination of crack locations, type and orientation in concrete structures by acoustic emission", *Mag. Concrete Res.*, **43**(155), 127-134.
- Ouyang, C., Landis, E. and Shah, S. (1991), "Damage assessment in concrete using quantitative acoustic emission", *J. Eng. Mech.*, **117**(11), 2681-2698.
- Raghu Prasad, B. and Vidya Sagar, R. (2008), "Relationship between AE energy and fracture energy of plain concrete beams: experimental study", *J. Mater. Civil Eng.*, **20**(3), 212-220.
- Vonk, R. (1993), "A micromechanical investigation of softening of concrete loaded in compression", *Herson*, **38**, 1-94.
- Wang, E. and Shrive, N. (1995), "Brittle fracture in compression: mechanisms, models and criteria", *Eng. Fract. Mech.*, **52**(6), 1107-1126.
- Watanabe, T., Nishibata, S., Hashimoto, C. and Ohtsu, M. (2007), "Compressive failure in concrete of recycled aggregate by acoustic emission", *Constr. Build. Mater.*, **21**, 470-476.